Photo-triggered spatially controlled out-of-equilibrium patterns of peptide nanofibers in a self-sorting double network hydrogel

Keisuke Nakamura[#a] , Wataru Tanaka[#a,d], Kei Sada[a], Ryou Kubota[a], Takuma Aoyama[b], Kenji Urayama[b] and Itaru Hamachi[*a,c]

[a]Department of Synthetic Chemistry and Biological Chemistry, Graduate School of Engineering, Kyoto University, Nishikyo-ku, Kyoto 615-8510, Japan

[b]Department of Macromolecular Science and Engineering, Kyoto Institute of Technology, Matsugasaki, Kyoto 606-8585, Japan

[c]JST-ERATO, Hamachi Innovative Molecular Technology for Neuroscience, Nishikyo-ku, Kyoto 615-8530, Japan

[d]Present address: Department of Applied Chemistry, Graduate School of Engineering, The University of Tokyo, Tokyo 113-8656, Japan

#These authors contributed equally to this work

*Corresponding Author: ihamachi@sbchem.kyoto-u.ac.jp

Abstract:

Out-of-equilibrium patterns arising from diffusion processes are ubiquitous in nature, although they have not been fully exploited for the design of artificial materials. Here, we describe the formation of photo-triggered out-of-equilibrium patterns using photo-responsive peptide-based nanofibers in a self-sorting double network hydrogel. Light irradiation using a photomask followed by thermal incubation induced the spatially controlled condensation of peptide nanofibers. According to confocal images and spectroscopic analyses, metastable nanofibers photo-decomposed in the irradiated areas, where thermodynamically stable nanofibers reconstituted and condensed with a supply of monomers from the non-irradiated areas. These supramolecular events were regulated by light and diffusion to facilitate the creation of unique out-of-equilibrium patterns, including two lines from a one-line photomask and a line pattern of a protein immobilized in the hydrogel.

Introduction

Living organisms generate a myriad of spatially periodic patterns, including dots, stripes, rings, spirals, and labyrinths, with sizes ranging from ~1 μm (*e.g.*, cellular signal transduction patterns) to 0.001–1 m (*e.g.*, skin patterns of vertebrate bodies)[1]. The concentration gradient of a morphogen, a molecule that interacts with neighboring cells (*e.g.*, growth factors), determines the position of biological patterns by driving protein expression and cell differentiation[2,3]. Various regulatory mechanisms are involved in the formation of the morphogen spatial gradient. For example, interactions with receptor proteins and the extracellular matrix suppress the diffusion of morphogens and feedback control affects the production and degradation of morphogens and signaling receptors[4,5]. The reaction-diffusion model can describe these experimental observations[6–8]. For example, this theoretical model was used to explain the spontaneous emergence of localized regions of morphogens through mutual interactions between two morphogens under the far-from-equilibrium reaction conditions to form steady-state dot/stripe patterns. Similar diffusion-coupled reactions produce out-of-equilibrium patterns that play central roles in sophisticated spatial self-organization, including embryogenesis and neuronal network formation[9,10].

Out-of-equilibrium patterns exist in the abiotic world[11,12]. For example, the Liesegang ring is the most representative stationary pattern to arise from a diffusion-dependent precipitation reaction[13]. These periodic band/ring patterns form *via* diffusion processes coupled with the nonlinear precipitation of complementary electrolytes (*e.g.*, potassium dichromate and silver nitrate). Therefore, diffusion-coupled reactions have attracted considerable attention for the creation of biomimetic out-of-equilibrium structures in synthetic self-assembled materials[14–21]. Recent studies have demonstrated that precipitation-based spatial patterning can be applied to surface-modified nanoparticles[22], polymer gels[23], and supramolecular assemblies[24–26]. Indeed, these reactions are potentially powerful for the fabrication of hierarchical materials from nano-sized building blocks, although these bottom-up approaches

are limited in design flexibility and synthesis controllability. Therefore, a development objective is the control of elaborate and life-like out-of-equilibrium stationary patterns using supramolecular assemblies *via* their reaction-diffusion processes involving feedback regulation. If diffusion-dependent out-of-equilibrium patterns can be triggered by external stimuli, such as light, then the resultant patterns can be precisely controlled in a spatiotemporal manner depending on the size, shape, and order of the stimuli. Such efforts remain challenging to date[27].

In this study, we demonstrated the photo-triggered formation of out-of-equilibrium patterns using peptide-type nanofibers in a self-sorting supramolecular double network (SDN) hydrogel[28,29]. In the SDN hydrogel comprising lipid- and peptide-type nanofibers, the peptide fibers were modified with acylhydrazone to serve as a photoswitch using a post-assembly fabrication (PAF) protocol[30]. Confocal laser scanning microscopic (CLSM) images[31,32] revealed that the peptide-type nanofibers photo-decomposed through *E*-to-*Z* isomerization and subsequently reformed *via* thermally induced *Z*-to-*E* transformation. Further incubation provided an unexpected discovery, that is, the spatial condensation of peptide-type nanofibers in the photo-irradiated areas and concurrent nanofiber depletion in the non-irradiated areas (Figure 1a). In-depth analyses indicated that the reconstructed peptide nanofibers were thermodynamically stable and seed-driven nanofiber condensation was enhanced by monomers diffusing from the kinetically trapped metastable nanofibers prepared by PAF. Complex unique patterns were constructed from simple photomasks using the present photo/diffusion-coupled out-of-equilibrium system, namely two-line patterns from a one-line photomask and grid-like patterns from a one-line photomask by consecutive photo-irradiation. Furthermore, spatially controlled patterning of proteins without photo-responsive properties embedded in this SDN hydrogel was also successful.

Results and discussion

Design strategy for a photo/thermally responsive SDN hydrogel

SDN hydrogels are promising as scaffolds for the rational integration of supramolecular nanofibers that are responsive to multiple stimuli[28–30,33–37]. Therefore, the patterning of SDN hydrogels offers the possibility to control multiple functions in a spatially resolved manner[38]. While the irreversible formation and degradation of photo-responsive nanofibers have been demonstrated[39–41], the reversible formation of nanofibers in SDN gels has not been achieved to date. We previously reported that a benzaldehyde-tethered peptide-type gelator (**Ald-F(F)F(F)**) and a lipid-type gelator (**Phos-cycC_6**) orthogonally self-assembled to form an SDN hydrogel (Figure 1b)[42]. Using this network as a template, we installed a photo-responsive module onto the aldehyde terminal of the peptide fiber using a PAF protocol[30,43]. The addition of a benzhydrazide solution generates a benzoylhydrazone group, a reversible photoswitch, in the peptide-type gel fiber (**BHz-F(F)F(F)**) without perturbing the SDN structure[44–46]. The *E* isomer of benzoylhydrazone transforms into the *Z* isomer under UV irradiation, and the *Z* isomer thermally reverts back into the *E* isomer by incubation under darkness at room temperature (rt). If the *Z*-form disturbs the packing mode of the peptide fiber, then the fibers may destabilize and thermally reform[46]. When photo-irradiation is conducted using a photomask, the peptide-type nanofibers are selectively destroyed in the limited exposed area, and subsequent incubation under darkness causes the nanofibers to reconstruct in the same area. Because the lipid-type fiber is not photo-responsive, these fibers serve as the intact gel matrix.

Prior to the construction of the SDN hydrogel, we first confirmed the photo-and-thermal (photo/thermal) responsiveness of a single component **BHz-F(F)F(F)** hydrogel prepared using the PAF protocol. A benzhydrazide solution added to the **Ald-F(F)F(F)** hydrogel followed by an incubation period (8 h) converted 95% of the **Ald-F(F)F(F)** gelator to **BHz-F(F)F(F)** in a macroscopic hydrogel (Figure S1 to S3)[47]. UV irradiation (325 nm LED, 2 h) converted the transparent hydrogel of **BHz-F(F)F(F)** into a partial gel and subsequent incubation for 24 h under darkness at rt resulted in a recovered gel. The photo-induced *E*-to-*Z*

isomerization of the benzoylhydrazone moiety was monitored with UV/vis spectral changes, that is, the appearance of the absorbance at 378 nm characteristic of the *Z*-form along with a decrease in the absorbance at 316 nm arising from the *E*-form (Figure 1c and S4). According to the increased absorbance at 378 nm and the NMR study, 12% of **BHz-F(F)F(F)** was photo-converted into the *Z* isomer (Figure S5). The thermal *Z*-to-*E* transformation was also examined by measuring UV/vis spectra, from which the half-life of the *Z* isomer (*ca.* 1 h) was determined (Figure 1d and S4). CLSM images of the peptide fibers of **BHz-F(F)F(F)** were obtained using a fluorescent probe, **NP-Alx647**, that co-assembled with this gelator (Figure S6). The as-prepared **BHz-F(F)F(F)** hydrogel comprised well-entangled fibers (Figure S7a). Upon UV irradiation, most of the long nanofibers disappeared and a few fragmented and unstructured aggregates were observable (Figure S7b). As expected, most of the entangled nanofibers regenerated after subsequent incubation under darkness (Figure S7c). These results clearly revealed that the photo-generated *Z* isomer, even in a small amount, perturbed the ordered packing of the self-assembled **BHz-F(F)F(F)** fibers and thermal *Z*-to-*E* isomerization reversibly repaired the ordered packing of the peptide-type gelators[46].

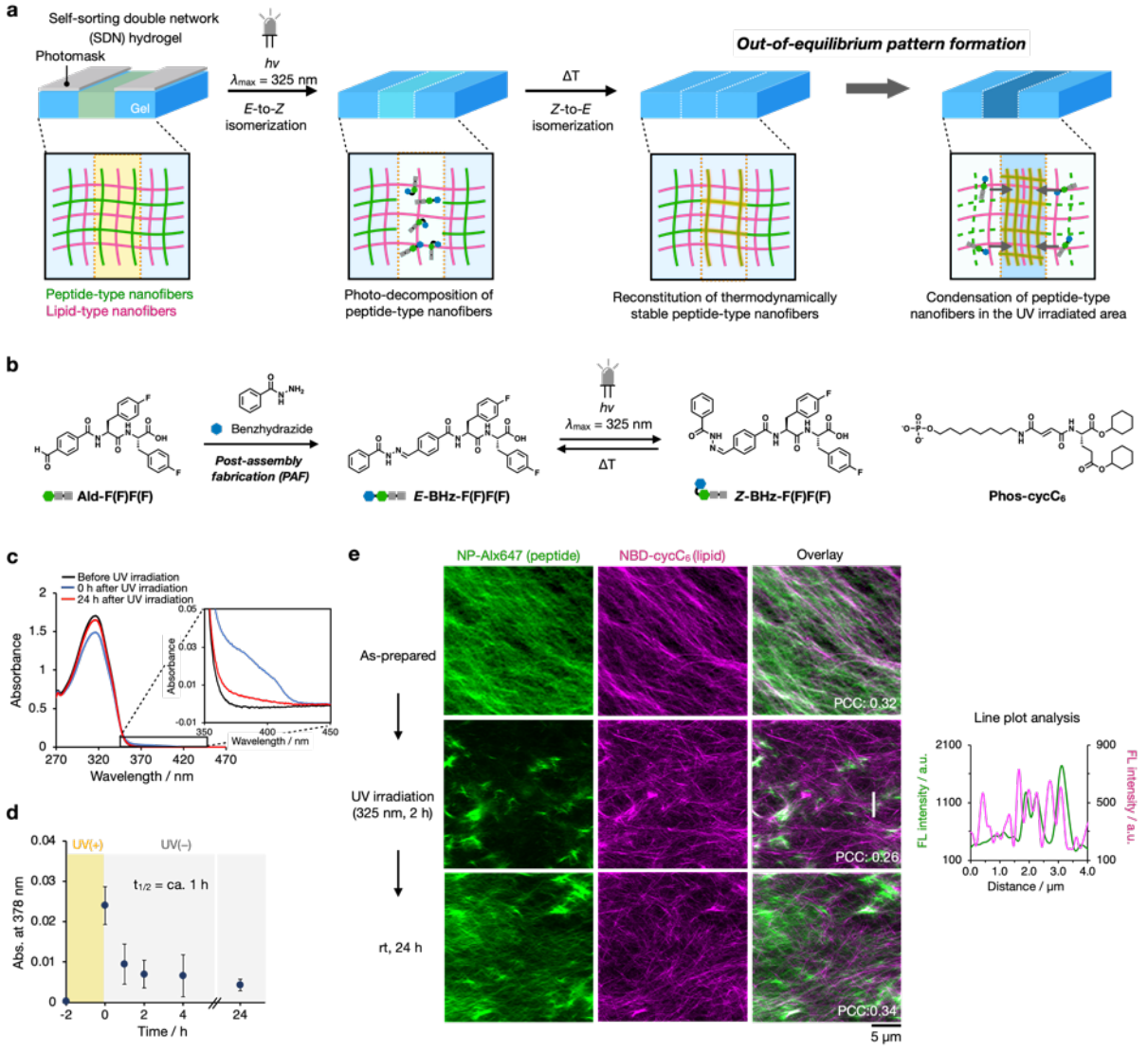

Figure 1. Schematic representation of out-of-equilibrium pattern formation and design of a photo/thermally responsive SDN hydrogel. (**a**) Photo-triggered out-of-equilibrium pattern using peptide-type nanofibers in the self-sorting supramolecular double network (SDN) hydrogel. (**b**) Chemical structures of the peptide-type gelator (**Ald-F(F)F(F)**/**BHz-F(F)F(F)**) and lipid-type gelator (**Phos-cycC$_6$**). (**c**) UV/vis spectra of the **BHz-F(F)F(F)** hydrogel before (black line) and after photo-irradiation (blue line) and after subsequent incubation under darkness (red line). The spectra were obtained after 177-fold dilution of the hydrogels with DMSO. (**d**) Time course of the absorbance at 378 nm before and after photo-irradiation. The data represent the mean ± standard deviation (n = 3). (**e**) High resolution Airyscan CLSM images of the SDN hydrogels (top) as-prepared and (middle) immediately after photo-

irradiation (325 nm, 2 h), and (bottom) after thermal incubation. Green: **NP-Alx647**, magenta: **NBD-cycC$_6$**. Scale bar: 5 μm. Line plot analysis along the white lines are shown on the right side of the images. PCC: Pearson's correlation coefficient, FL intensity: fluorescence intensity. Conditions: [**Ald-F(F)F(F)**] = 0.5 wt% (10.4 mM), [benzhydrazide] = 20.8 mM, [**Phos-cycC$_6$**] = 1.0 wt% (16.3 mM) (for **e**), [**NP-Alx647**] = 4 μM (for **e**), [**NBD-cycC$_6$**] = 20 μM (for **e**), 100 mM MES buffer (pH 7.0), rt.

Post-assembly fabrication of a photo/thermally responsive SDN hydrogel

Having characterized the photo/thermally responsive **BHz-F(F)F(F)** nanofiber, we subsequently constructed the SDN hydrogel using the PAF protocol. The lipid-type nanofiber **Phos-cycC$_6$** was not susceptible to UV (325 nm) irradiation (Figure S8). A suspended mixture of **Ald-F(F)F(F)** and **Phos-cycC$_6$** in 100 mM MES buffer solution (pH 7) was heated until dissolving and then cooled to rt to form a hydrogel (Figure S9a and S10). Benzhydrazide was added to this hydrogel followed by 12 h of incubation, thus producing an SDN hydrogel comprising two components (**BHz-F(F)F(F)/Phos-cycC$_6$**) (Figure S9a). HPLC analysis indicated that 99% of **Ald-F(F)F(F)** was converted into **BHz-F(F)F(F)**, whereas **Phos-cycC$_6$** was unaffected (Figure S9b). The SDN structure of the two distinct fibers before and after the benzhydrazide treatment was evaluated with CLSM images obtained using two different fluorescent probes, **NP-Alx647** and **NBD-cycC$_6$**, which contained a self-assembled motif similar to the peptide-type gelators (**Ald-F(F)F(F)**/**BHz-F(F)F(F)**) and **Phos-cycC$_6$**, respectively (Figure 1e, S6, S11). The CLSM images of the hydrogel without benzhydrazide and their line plot analysis revealed the existence of interpenetrated self-sorted nanofibers of **Ald-F(F)F(F)** and **Phos-cycC$_6$**, which scarcely overlapped with each other (Figure S12). After the formation of **BHz-F(F)F(F)** by the addition of benzhydrazide, the **BHz-F(F)F(F)** nanofibers partially overlapped with the **Phos-cycC$_6$** nanofibers, and indeed Pearson's correlation coefficient increased from 0.07 to 0.32 (Figure 1e, top). This suggested that the

attached benzhydrazide moiety increased the hydrophobicity of the peptide-type gelator (Table S1), which enhanced their interactions with the lipid-type nanofibers, while the orthogonal network was almost maintained.

The photo/thermal responsiveness of the resultant SDN hydrogels was then evaluated by using CLSM imaging and UV/vis spectroscopy. In the CLSM image obtained immediately after photo-irradiation, many long **BHz-F(F)F(F)** fibers were absent, while the **Phos-cycC$_6$** nanofibers remained intact (Figure 1e, middle). Shortened and unstructured aggregates of the peptide-type nanofibers were observed, a few of which were co-localized within the lipid nanofiber mesh (Figure 1e, line plot), which suggested that the photo-insensitive lipid-type nanofiber network served as a reservoir to entrap the photo-fragmented peptide fibers. In the image obtained after the hydrogel was subsequently incubated under darkness for 24 h, the SDN structure was reproduced (Figure 1e, bottom), indicating that numerous long **BHz-F(F)F(F)** nanofibers were regenerated with little perturbation to the **Phos-cycC$_6$** network. Further evidence for the photo-induced *E*-to-*Z* isomerization of **BHz-F(F)F(F)** and the subsequent recovery of the *E*-form by thermal Z-to-*E* isomerization in the SDN hydrogel was provided by the UV/vis spectra (Figure S13). These results clearly indicated that the reversible photo/thermal responsiveness of the **BHz-F(F)F(F)** nanofibers was retained in the presence of the **Phos-cycC$_6$** nanofibers; specifically, morphological changes in the peptide-type assembly did not adversely affect the **Phos-cycC$_6$** network.

Photo-triggered spatially controlled out-of-equilibrium pattern of the SDN hydrogel

We next conducted photo-fabrication using a photomask on the SDN hydrogel containing the **BHz-F(F)F(F)** nanofibers and then examined the thermal recovery of the photo-patterned hydrogel (Figure 2a and Table S2). Before photo-irradiation, an almost homogeneous distribution of the two gelators was observed in the CLSM image obtained with a low-magnification objective lens (5×) (Figure 2b). Photo-irradiation using the photomask produced

dark lines, which was imaged by the Alx647 channel but was not detected by the NBD channel. Therefore, the **BHz-F(F)F(F)** hydrogel was selectively transformed in the areas exposed to UV irradiation, while the **Phos-cycC$_6$** nanofibers remained intact. As a result, a spatial pattern comprising multi-lines of the lipid-type network was constructed in the SDN hydrogel matrix. As shown in the high-magnification CLSM image, most of the long **BHz-F(F)F(F)** nanofibers disappeared in the irradiated areas, while the well-developed **Phos-cycC$_6$** nanofibers remained intact (Figure 2c and S14). A few of the fragmented peptide nanofibers were observed in the irradiated areas, and these fibers were partially entrapped within the lipid-type nanofibers. The photo-generated dark lines gradually disappeared during thermal incubation under darkness, and an almost homogenous image was restored in the Alx647 channel within 30 min after photo-irradiation, thus demonstrating the reversibility of photo-patterning on the SDN hydrogel, as we initially designed. (Figure 2b and 2c).

Unexpectedly, we noticed that the fluorescence of the UV-irradiated lines in the Alx647 channel increased and became stronger than the initial fluorescence with increasing incubation time (Figure 2b and Movie S1). A line plot analysis of the time-dependent CLSM images provided further information (Figure 2d and S15). After photo-irradiation (30 min), the fluorescence around the photo-irradiated areas was weaker than that within the non-irradiated areas. During thermal incubation, the bleached fluorescence in the UV-irradiated areas recovered and became stronger than the initial fluorescence. In contrast, in the non-irradiated area, the fluorescence was substantially weaker. In the high-magnification CLSM images, numerous long **BHz-F(F)F(F)** nanofibers were regenerated in the photo-irradiated areas (Figure 2c, 2e and S14, and Movie S2). Therefore, the dark gaps gradually accumulated fibers with fluorescence stronger than the initial fluorescence. In these areas, the overlapping **BHz-F(F)F(F)** and **Phos-cycC$_6$** nanofibers indicated the formation of a parallel SDN matrix. We thus concluded that the photo-triggered out-of-equilibrium pattern (5–100 μm) originated from the condensation of regenerated peptide nanofibers in the photo-irradiated areas of the SDN

hydrogel. Moreover, 3D imaging showed that the photo-degradation and the condensation of the peptide nanofibers occurred to a depth of ca. 200 μm from the photo-irradiated side (Figure S16).

Similar photo-triggered out-of-equilibrium line patterns were created with photomasks marked with varied line widths, namely 5, 10, and 20 μm (Figure S17 and S18). Interestingly, the recovery time of the Alx647 fluorescence intensity to the original value was dependent on the width, that is, recovery was rapid for the thinner line width[48]. The photo-triggered line pattern also emerged at higher temperature (37 °C), while the condensation proceeded more rapidly than rt (Figure S19). Both line width- and temperature-dependent experiments suggested that the pattern formation would depend on diffusion.

Photo patterns generated by spatial condensation have not been constructed using a single component **BHz-F(F)F(F)** hydrogel. The CLSM image of the **BHz-F(F)F(F)** hydrogel detected by the Alx647 channel and its line plot analysis showed that dark lines were initially produced in the irradiated areas upon photo-irradiation, similar to those of the SDN hydrogel (Figure 2f and S20). Subsequent thermal incubation, however, produced neither fluorescence recovery nor further intensification of the irradiated lines. Instead, the fluorescence outside the irradiated areas gradually diminished. The high-magnification CLSM images did not show any condensed peptide fibers in the irradiated areas (Figure S21 and Movie S3). Similarly, simple degradation of the photo-patterned lines occurred without condensation when we used a composite network of **BHz-F(F)F(F)** and agarose (Alx488-modified agarose, **Alx488-Agarose**, was used for imaging) (Figure S22 to S24). The densely meshed agarose hydrogel was reported to be orthogonally blended with the peptide-type nanofibers[49], and the agarose network did not provide any hydrophobic domains, unlike **Phos-cycC$_6$**. These two control experiments demonstrated that **Phos-cycC$_6$** in the SDN hydrogel suppressed the diffusion of the photo-fragmented **BHz-F(F)F(F)** fibers because of the interactions between the two gelators, which critically promoted the seed-driven reconstruction and enrichment of the

peptide nanofibers.

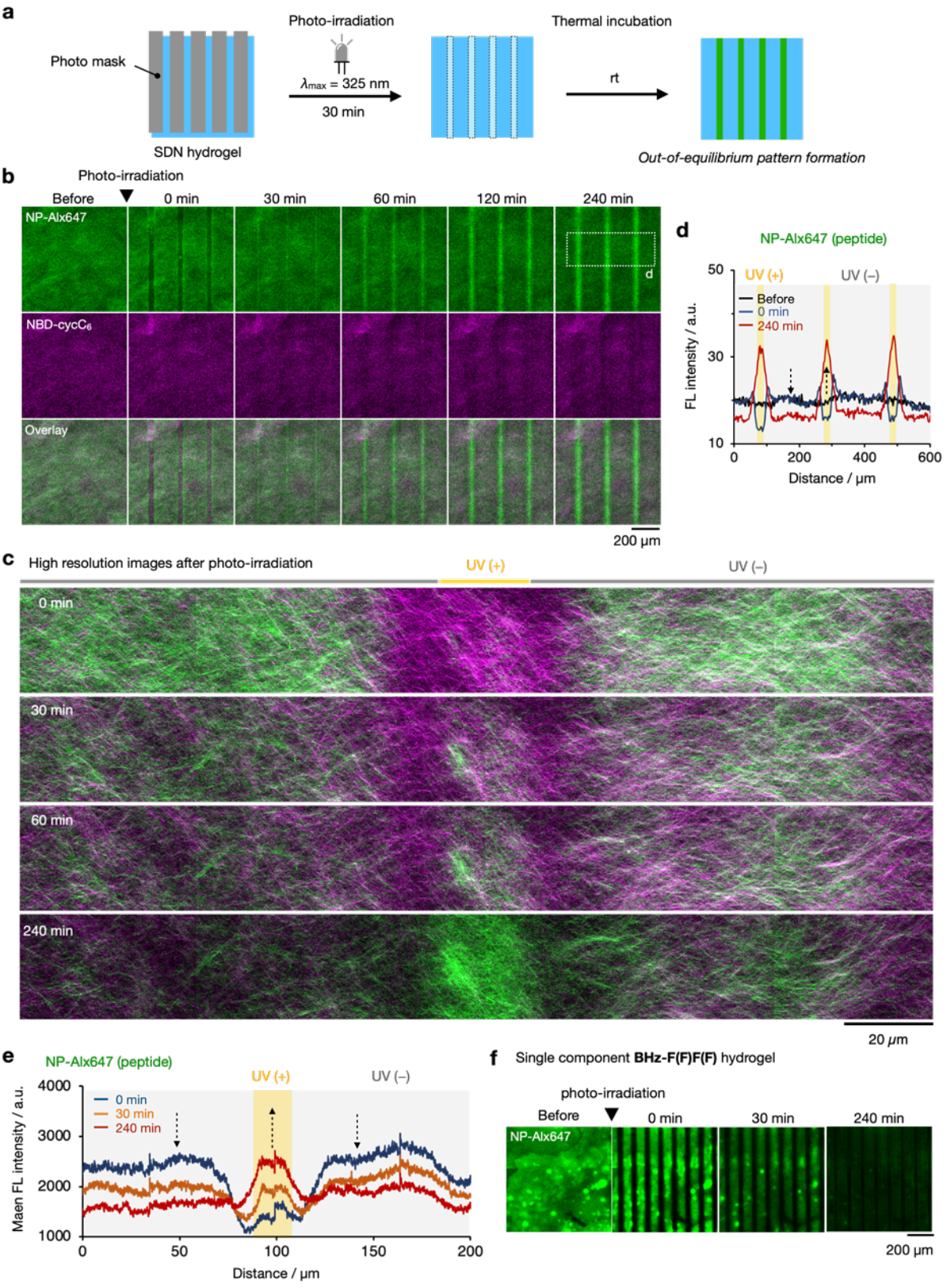

Figure 2. Photo-triggered out-of-equilibrium pattern formation. (**a**) Experimental setup for photo-irradiation with a photomask. (**b**) Time-lapse CLSM imaging of the **BHz-**

F(F)F(F)/Phos-cycC$_6$ hydrogel before and after photo-irradiation (325 nm, 30 min) using a photomask (line width: 20 μm, interval: 180 μm). Scale bar: 200 μm. (**c**) High resolution Airyscan CLSM imaging of the out-of-equilibrium pattern formation after photo-irradiation (325 nm, 30 min) using a photomask (line width: 20 μm, interval: 180 μm). (**d**) Line plot analysis of the mean FL intensity (Alx647 channel) at each coordinate along the horizontal axis of the white square shown in Figure 2**b**. Black line: before, blue line: 0 min after photo-irradiation, red line: 240 min after photo-irradiation. (**e**) Line plot analysis of the mean FL intensity (Alx647 channel) at each coordinate along the horizontal axis of Figure 2**c**. (**f**) Time-lapse CLSM images of the **BHz-F(F)F(F)** hydrogel before and after photo-irradiation (325 nm, 30 min) using a photomask (line width: 10 μm, interval: 90 μm). Scale bar: 200 μm. Conditions: [**Ald-F(F)F(F)**] = 0.5 wt% (10.4 mM), [benzhydrazide] = 20.8 mM, [**Phos-cycC$_6$**] = 1.0 wt% (16.3 mM) (for **a**-**e**), [**NP-Alx647**] = 4 μM, [**NBD-cycC$_6$**] = 20 μM (for **a**-**e**), 100 mM MES buffer (pH 7.0), rt.

Formation mechanism of the out-of-equilibrium pattern in SDN hydrogel

On the basis of our experimental results, we postulated that the formation of the photo-triggered and thermally recovered patterns included the following three main steps: (i) spatially limited decomposition of the peptide-type nanofibers in the photo-irradiated areas by photo-induced *E*-to-*Z* isomerization of the **BHz-F(F)F(F)** gelator; (ii) partially suppressed diffusion of the photo-fragmented **BHz-F(F)F(F)** fibers within the **Phos-cycC$_6$** nanofiber network of the SDN hydrogel; and (iii) reconstruction of the **BHz-F(F)F(F)** nanofibers in the photo-irradiated areas through thermal *Z*-to-*E* isomerization and consequent reassembly. It was not clear how the condensation of the **BHz-F(F)F(F)** nanofibers was induced during the prolonged thermal incubation for the generation of this out-of-equilibrium pattern.

Circular dichroism (CD) spectroscopy of the **BHz-F(F)F(F)** hydrogels provided information for the elucidation of this condensation event. The CD spectrum of the *in situ* as-

prepared **BHz-F(F)F(F)** fibers *via* PAF contained negative Cotton peaks at 204, 276, and 344 nm with weak ellipticity (Figure 3a, black). Photo-irradiation followed by thermal incubation yielded a significantly altered spectrum containing new strong peaks at 265 (positive) and 296 (negative) nm (Figure 3a red, S25 and S26), indicating that the packing mode of **BHz-F(F)F(F)** in the reconstructed hydrogel was different from that of the as-prepared hydrogel. More importantly, almost the same CD spectral shape was obtained by thermally annealing (from 20 to 90 °C at a rate of 2 °C/min) the as-prepared **BHz-F(F)F(F)** hydrogels (Figure 3a, yellow). In addition, the CD spectrum of the photo/thermally reconstructed hydrogel was scarcely changed by heat treatment even at 90 °C (Figure S25 and S26). Therefore, the as-prepared **BHz-F(F)F(F)** nanofibers were metastable and the reconstructed fibers were thermodynamically stable.

Because of the PAF protocol, the packing of the **Ald-F(F)F(F)** template nanofibers strongly affected the packing mode of the as-prepared **BHz-F(F)F(F)** nanofibers, which promoted the generation of kinetically trapped metastable fibers (Figure S27). According to previous reports, when two different supramolecular assemblies comprising the same monomer dynamically coexist, the more stable supramolecular polymer can preferentially grow from the disassembled monomer of the less stable polymer[50–52]. In our SDN hydrogel, photo-irradiation followed by thermal incubation destroyed the metastable as-prepared **BHz-F(F)F(F)** fibers, and thermodynamically stable fibers were reconstructed predominantly in the photo-irradiated areas (Figure 3b). The seeds of the thermodynamically stable fibers were provided by the fragmented **BHz-F(F)F(F)** fibers retained in these areas. However, the as-prepared peptide fibers in the non-irradiated areas were dynamically destabilized by the *E*/*Z* monomeric and/or oligomeric **BHz-F(F)F(F)** diffusing from the photo-irradiated areas. Under these spatially limited dynamic conditions, monomeric **BHz-F(F)F(F)** was supplied by metastable as-prepared peptide fibers for the construction of thermodynamically stable **BHz-F(F)F(F)** fibers. Therefore, prolonged incubation facilitated the elongation and enrichment of the reconstructed

peptide fibers in the photo-irradiated area. Indeed, we noticed that the areas containing the condensed **BHz-F(F)F(F)** fibers were slightly extended from the line width of the photomask because these dynamic areas support diffusion-dependent fibers decomposition/rearrangement (Figure 2c and 2e).

To further validate the mechanism, we investigated whether the metastable nanofibers are essential for the out-of-equilibrium pattern formation. We initially converted the metastable peptide nanofibers to the thermodynamically stable ones by photo-irradiation to the whole area of the SDN hydrogels followed by incubation at rt. The reconstituted hydrogel was then irradiated using a photomask (line width: 20 μm). CLSM imaging showed that the decomposition of the peptide nanofibers occurred at the photo-irradiated area; however, the regeneration of the peptide nanofibers never be observed (Figure 3c and S28). These results suggested that supply of peptide monomers from the thermodynamically stable nanofibers was largely suppressed. On the other hand, the fluorescence intensity at the outer edge of the photo-irradiated area was significantly increased, indicating that the photo-decomposed peptide monomers/aggregates diffused and reformed there. These results strongly supported our proposed mechanism of the out-of-equilibrium pattern formation.

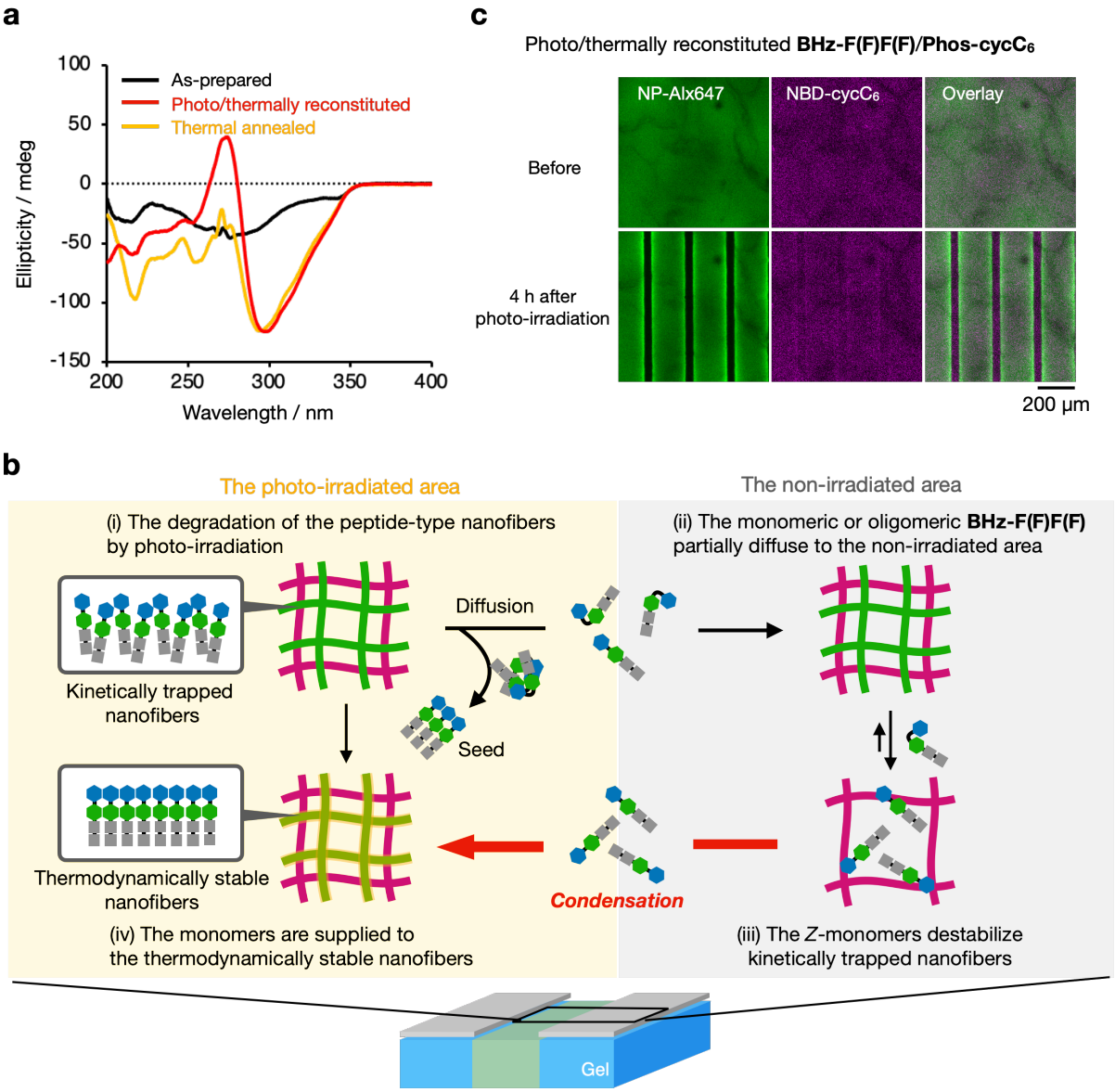

Figure 3. Plausible formation mechanism of the out-of-equilibrium pattern. (**a**) CD spectra of the **BHz-F(F)F(F)** hydrogel before and after photo-irradiation. Black line: as-prepraed, red line: photo/thermal reconstituted, yellow line: thermal annealed. (**b**) Expected mechanism of the out-of-equilibrium pattern formation in the SDN hydrogel. (**c**) CLSM imaging of the photo/thermally reconstituted **BHz-F(F)F(F)/Phos-cycC$_6$** hydrogel before and after photo-irradiation (325 nm, 30 min) using a photomask (line width: 20 μm, interval: 180 μm) followed by thermal incubation. Scale bar: 200 μm. Conditions: [**Ald-F(F)F(F)**] = 0.5 wt% (10.4 mM),

[benzhydrazide] = 20.8 mM, [**Phos-cycC$_6$**] = 1.0 wt% (16.3 mM) (for **c**), [**NP-Alx647**] = 4 μM (for **c**), [**NBD-cycC$_6$**] = 20 μM (for **c**), 100 mM MES buffer (pH 7.0), rt.

Unique photo-triggered patterns due to the out of equilibrium

Using this SDN hydrogel in which photo-activation promotes seed-driven supramolecular polymerization controlled by diffusion, we finally created unprecedented out-of-equilibrium patterns that cannot be constructed from conventional photo-fabrication materials. First, double lines were formed within a single UV-irradiated line using a photomask marked with a wide line (40 μm) (Figure 4a and S29). As shown in Figure 4a, two strong fluorescence lines were observed proximal to both edges of the irradiated area and the relatively weak fluorescence was observed along the line center (Figure 4b). Therefore, the diffusion and polymerization of **BHz-F(F)F(F)** monomers from the non-irradiated areas was faster to the edge than to the center of the photo-irradiated area.

Second, consecutive UV-irradiation using two distinct arrangements of the photomask produced a unique grid-like pattern. The first photo-irradiation was followed by thermal incubation for 10 h, and the second irradiation was conducted with a 90° rotation of the same photomask followed by thermal incubation of the SDN hydrogel in the dark. A grid-like pattern generated through this photo-thermal fabrication protocol was imaged by the Alx647 channel (Figure 4c and S30). Remarkably, double fluorescence bands were clearer along the horizontal direction than along the vertical direction (Figure 4d and 4e). This unique pattern was formed because the supply of **BHz-F(F)F(F)** monomers differed between the first and second irradiation. During the first photo-irradiation, a sufficient amount of peptide gelator diffused into the irradiated areas and a relatively small amount of peptide gelator remained in the non-irradiated areas. For the second photo-irradiation, **BHz-F(F)F(F)** monomers were in lower supply, and **BHz-F(F)F(F)** mostly condensed at the edge of the horizontal lines.

Photo-triggered out-of-equilibrium pattern formation is not limited to photo-

responsive peptide gelators. A fluorescent-labeled protein (TMR-streptavidin, TMR: tetramethylrhodamine) was embedded in this SDN hydrogel. The high-magnification CLSM images visualized that TMR-streptavidin were well overlapped with the **BHz-F(F)F(F)** nanofibers (Pearson's correlation coefficient: 0.73), but not with the **Phos-cycC_6** nanofibers (Pearson's correlation coefficient: 0.18) (Figure S31). These data indicated that TMR-streptavidin preferentially interacted with the peptide nanofibers rather than the lipid nanofibers. We subsequently conducted photo-irradiation using a photomask followed by thermal incubation for 4 h (Figure 4f to 4h and S32). The line pattern constructed *via* a condensation of streptavidin was detected by the TMR channel, as shown in Figure 4g. Importantly, this pattern and that of the condensed **BHz-F(F)F(F)** fibers (Alx647 channel) matched in the overlay image (Figure 4h), clearly demonstrating that optically activated condensation of a protein molecule (unresponsive to UV irradiation) based on this out-of-equilibrium phenomenon was successful. Although the constituents of the SDN hydrogel are much simpler than those of living organisms, the interplay of photo-activation, kinetic trapping, and diffusion-controlled aggregation in the present supramolecular assembly can facilitate the rational design of synthetic materials with spatiotemporally controlled hierarchical structures and functions. We anticipate that the out-of-equilibrium pattern formation presented here could be extended to a three-dimensional patterning technique with the aid of photo-triggered molecular/supramolecular diffusion, which proceeds in three dimensions even if a 2D photomask is used. Such a research direction is currently underway.

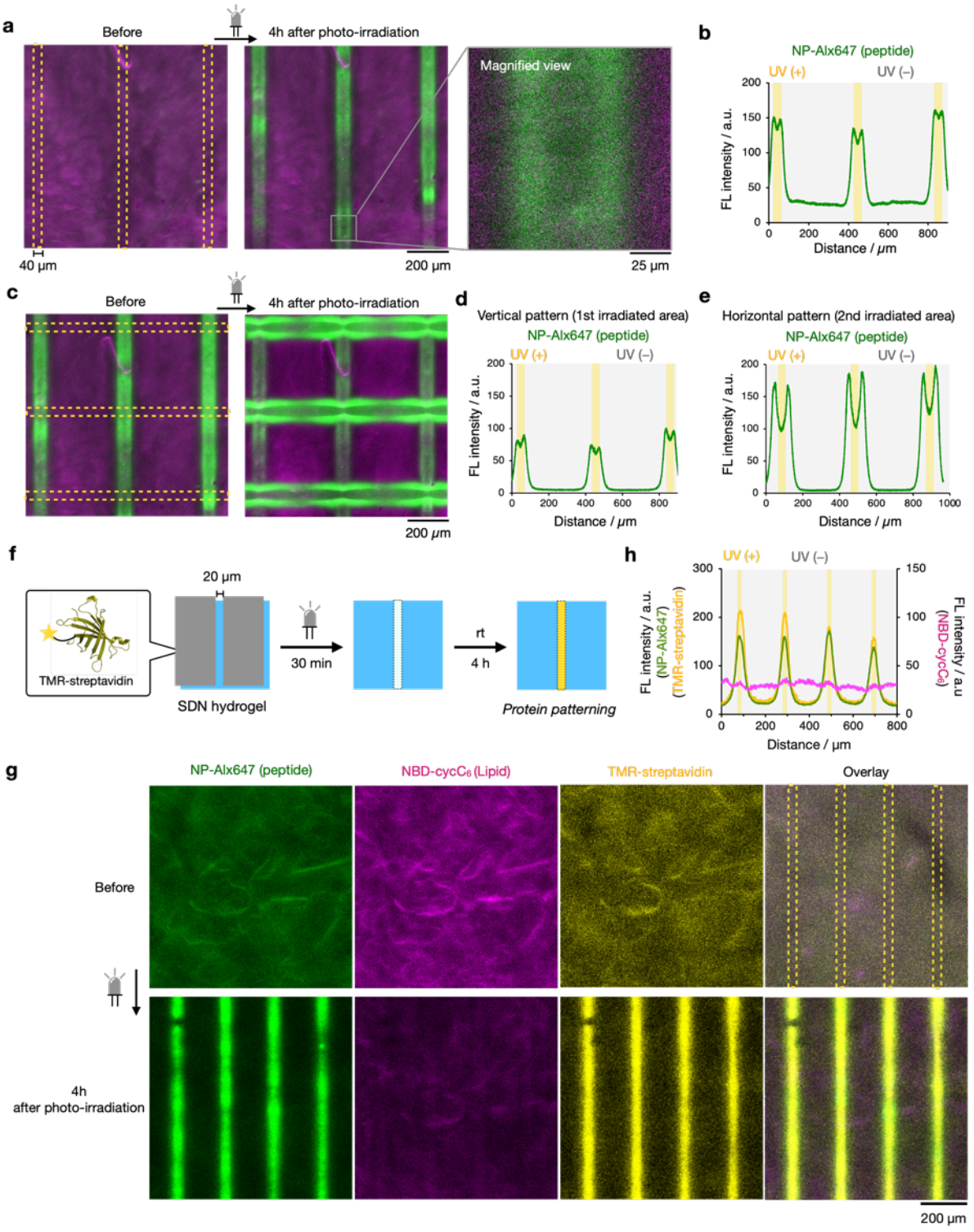

Figure 4. Unique pattern formation. (**a**) CLSM imaging of the **BHz-F(F)F(F)/Phos-cycC$_6$** hydrogel before and 4 h after photo-irradiation (325 nm, 30 min) using a wide photomask (line width: 40 μm, interval: 360 μm). (**b**) Line plot analysis of the mean FL intensity (Alx647 channel). Region of interests were shown in Figure S29. (**c**) CLSM imaging of the pre-

patterned **BHz-F(F)F(F)/Phos-cycC_6** hydrogel before and 4h after 2nd photo-irradiation (325 nm, 30 min) using a wide photomask (line width: 40 μm, interval: 360 μm). (**d, e**) Line plot analysis of the mean FL intensity (Alx647 channel). Region of interests were shown in Figure S30. (**f**) Experimental setup for protein patterning. (**g**) CLSM imaging of the **BHz-F(F)F(F)/Phos-cycC_6** hydrogel containing TMR-streptavidin before and 4 h after photo-irradiation (325 nm, 30 min) using a photomask (line width: 20 μm, interval: 180 μm). TMR: tetramethylrhodamine. (**h**) Line plot analysis of the mean FL intensity at each coordinate along the horizontal axis of Figure 4**g**. Conditions: [**Ald-F(F)F(F)**] = 0.5 wt% (10.4 mM), [benzhydrazide] = 20.8 mM, [**Phos-cycC_6**] = 1.0 wt% (16.3 mM), [**NP-Alx647**] = 4 μM, [**NBD-cycC_6**] = 20 μM, [TMR-streptavidin] = 0.1 mg/mL (3.2 dye per protein) (for **f-h**), 100 mM MES buffer (pH 7.0), rt, yellow dashed square: photo-irradiated area. Scale bar: 200 μm.

References

1. Whitesides, G. M.; Grzybowski, B. Self-assembly at all scales. *Science* **2002**, *295*, 2418–2421.
2. Lander, A. D. Morpheus unbound: reimagining the morphogen gradient. *Cell* **2007**, *128*, 245–256.
3. Kondo, S.; Miura, T. Reaction-diffusion model as a framework for understanding biological pattern formation. *Science* **2010**, *329*, 1616–1620.
4. Li, P.; Markson, J. S.; Wang, S.; Chen, S.; Vachharajani, V.; Elowitz, M. B. Morphogen gradient reconstitution reveals Hedgehog pathway design principles. *Science,* **2018**, *360*, 543–548.
5. Toda, S.; McKeithan, W. L.; Hakkinen, T. J.; Lopez, P.; Klein, O. D.; Lim, W.A.. Engineering synthetic morphogen systems that can program multicellular patterning. *Science* **2020**, *370*, 327–331.

6. Turing, A. M. The chemical basis of morphogenesis. *Phil. Trans. R. Soc.* **1957**, *B237*, 37–72.
7. Kondo, S.; Asal, R. A reaction-diffusion wave on the skin of the marine angelfish Pomacanthus. *Nature* **1995**, *376*, 765–768.
8. Soh, S.; Byrska, M.; Kandere-Grzybowska, K.; Grzybowski, B. A. Reaction-diffusion systems in intracellular molecular transport and control. *Angew. Chem. Int. Ed.* **2010**, *49*, 4170–4198.
9. Gregor, T.; Tank, D. W.; Wieschaus, E. F.; Bialek, W. Probing the limits to positional information. *Cell* **2007**, *130*, 153–164.
10. Linville, A.; Radtke, K.; Waxman, J. S.; Yelon, D.; Schilling, T. F. Combinatorial roles for zebrafish retinoic acid receptors in the hindbrain, limbs and pharyngeal arches. *Dev. Biol.* **2009**, *325*, 60–70.
11. Grzybowski, B. A.; Huck, W. T. S. The nanotechnology of life-inspired systems. *Nat. Nanotechnol.* **2016**, *11*, 585–592.
12. Epstein, I. R.; Xu, B. Reaction-diffusion processes at the nano- and microscales. *Nat. Nanotechnol.* **2016**, *11*, 312–319.
13. Nakouzi, E.; Steinbock, O. Self-organization in precipitation reactions far from the equilibrium. *Sci. Adv.* **2016**, *2*, e1601144.
14. Carnall, J. M. A.; Waudby, C. A.; Belenguer, A. M.; Stuart, M. C. A.; Peyralans, J. J.-P.; Otto, S. Mechanosensitive self-replication driven by self-organization. *Science* **2010**, *327*, 1502–1506.
15. Padirac, A.; Fujii, T.; Estévez-Torres, A.; Rondelez, Y. Spatial waves in synthetic biochemical networks. *J. Am. Chem. Soc.* **2013**, *135*, 14586–14592.
16. Pappas, C. G.; Sasselli, I. R.; Ulijn, R. V. Biocatalytic pathway selection in transient tripeptide nanostructures. *Angew. Chem. Int. Ed.* **2015**, *54*, 8119–8123.
17. Boekhoven, J.; Hendriksen, W. E.; Koper, G. J. M.; Eelkema, R.; van Esch, J. H. Transient

assembly of active materials fueled by a chemical reaction. *Science* **2015**, *349*, 1075–1079.

18. Tena-Solsona, M.; Rieß, B.; Grötsch, R. K.; Löhrer, F. C.; Wanzke, C.; Käsdorf, B.; Bausch, A. R.; Müller-Buschbaum, P.; Lieleg, O.; Boekhoven, J. Non-equilibrium dissipative supramolecular materials with a tunable lifetime. *Nat. Commun.* **2017**, *8*, 15895.
19. Leira-Iglesias, J.; Tassoni, A.; Adachi, T.; Stich, M.; Hermans, T. M. Oscillations, travelling fronts and patterns in a supramolecular system. *Nat. Nanotechnol.* **2018**, *13*, 1021–1027.
20. Kubota, R.*;* Makuta, M.; Suzuki, R.; Ichikawa, M.; Tanaka, M.; Hamachi, I. Force generation by a propagating wave of supramolecular nanofibers. *Nat. Commun.* **2020,** *11*, 3541.
21. Panja, S.; Dietrich, B.; Adams, D. J. Chemically fuelled self-regulating Gel-to-Gel Transition. *ChemSystemsChem* **2020**, *2*, e190003.
22. Lagzi, I.; Kowalczyk, B.; Grzybowski, B. A. Liesegang rings engineered from charged nanoparticles. *J. Am. Chem. Soc.* **2010**, *132*, 58–60.
23. Narita, T.; Tokita, M. Liesegang pattern formation in κ-carrageenan gel. *Langmuir* **2006**, *22*, 349–352.
24. de Jong, J. J. D.; Hania, P. R.; Pugžlys, A.; Lucas, L. N.; de Loos, M.; Kellogg, R. M.; Feringa, B. L.; Duppen, K.; van Esch, J. H. Light-driven dynamic pattern formation. *Angew. Chem. Int. Ed.* **2005**, *44*, 2373–2376.
25. Lovrak, M.; Hendriksen, W. E. J.; Maity, C.; Mytnyk, S.; van Steijin, V.; Eelkema, R.; van Esch, J. H. Free-standing supramolecular hydrogel objects by reaction-diffusion. *Nat. Commun.* **2017**, *8*, 15317.
26. Schlichter, L.; Piras, C. C.; Smith, D. K. Spatial and temporal diffusion-control of dynamic multi-domain self-assembled gels. *Chem. Sci.* **2021**, *12*, 4162–4172.
27. Bensemann, I. T.; Fialkowski, M.; Grzybowski, B. A. Wet stamping of microscale periodic

precipitation patterns. *J. Phys. Chem. B* **2005**, *109*, 2774–2778.

28. Onogi, S.; Shigemitsu, H.; Yoshii, T.; Tanida, T.; Ikeda, M.; Kubota, R.; Hamachi, I. In situ real-time imaging of self-sorted supramolecular nanofibres. *Nat. Chem.* **2016**, *8*, 743–752.
29. Shigemitsu, H.; Fujisaku, T.; Tanaka, W.; Kubota, R.; Minami, S.; Urayama, K.; Hamachi, I. An adaptive supramolecular hydrogel comprising self-sorting double nanofibre networks. *Nat. Nanotechnol.* **2018**, *13*, 165–172.
30. Tanaka, W.; Shigemitsu, H.; Fujisaku, T.; Kubota, R.; Minami, S.; Urayama, K.; Hamachi, I. Post-assembly fabrication of a functional multicomponent supramolecular hydrogel Based on a self-sorting double network. *J. Am. Chem. Soc.* **2019**, *141*, 4997–5004.
31. Pujals, S.; Feiner-Gracia, N.; Delcanale, P.; Voets, I.; Albertazzi, L. Super-resolution microscopy as a powerful tool to study complex synthetic materials. *Nat. Rev. Chem.* **2019**, *3*, 68–84.
32. Kubota, R.; Tanaka, W.; Hamachi, I. Microscopic imaging techniques for molecular assemblies: Electron, atomic force, and confocal microscopies. *Chem. Rev.* **2021** doi:10.1021/acs.chemrev.0c01334.
33. Sugiyasu, K.; Kawano, S.-I.; Fujita, N.; Shinkai, S. Self-sorting organogels with p－n heterojunction points. *Chem. Mater.* **2008**, *20*, 2863–2865.
34. Moffat, J. R.; Smith, D. K. Controlled self-sorting in the assembly of "multi-gelator" gels. *Chem. Commun.* **2009**, 316–318.
35. Boekhoven, J.; Koot, M.; Wezendonk, T. A.; Eelkema, R.; van Esch, J. H. A self-assembled delivery platform with post-production tunable release rate. *J. Am. Chem. Soc.* **2012**, 134, 12908–12911.
36. Morris, K. L. Chen, L.; Raeburn, J.; Sellick, O. R.; Cotanda, P.; Paul, A.; Griffiths, P. C.; King, S. M.; O'Reilly, R. K.; Serpell, L. C.; Adams, D. J. Chemically programmed self-sorting of gelator networks. *Nat. Commun.* **2013**, *4*, 1480.

37. Sarkar, A.; Sasmal, R.; Empereur-mot, C.; Bochicchio, D.; Kompella, S. V. K.; Sharma, K.; Dhiman, S.; Sundaram, B.; Agasti, S. S.; Pavan, G. M.; George, S. J. Self-sorted, random, and block supramolecular copolymers via sequence controlled, multicomponent self-assembly. *J. Am. Chem. Soc.* **2020**, *142*, 7606–7617.
38. Chivers, P. R. A.; Smith, D. K. Shaping and structuring supramolecular gels. *Nat. Rev. Mater.* **2019**, *4*, 463–478.
39. Draper, E. R.; Eden, E. G. B.; McDonald, T. O.; Adams, D. J. Spatially resolved multicomponent gels. *Nat. Chem.* **2015**, *7*, 848–852.
40. Cornwell, D. J.; Daubney, O. J.; Smith, D. K. Photopatterned multidomain gels: multi-component self-assembled hydrogels based on partially self-sorting 1,3:2,4-dibenzylidene-D-sorbitol derivatives. *J. Am. Chem. Soc.* **2015**, *137*, 15486–15492.
41. Che, X.; Bai, B.; Zhang, T.; Zhang, C.; Zhang, C.; Zhang, P.; Wang, H.; Li, M. Gelation behaviour and gel properties of two-component organogels containing a photoresponsive gelator. *New J. Chem.* **2017**, *41*, 8614–8619.
42. Kubota, R.; Nagao, K.; Tanaka, W.; Matsumura, R.; Aoyama, T.; Urayama, K.; Hamachi, I. Control of seed formation allows two distinct self-sorting patterns of supramolecular nanofibers. *Nat. Commun.* **2020**, *11*, 4100.
43. Fernández-Castaño Romera, M.; Lou, X.; Schill, J.; ter Huurne, G.; Fransen, P.-P. K. H.; Voets, I. K.; Storm, C.; Sijbesma, R. P. Strain-stiffening in dynamic supramolecular fiber networks. *J. Am. Chem. Soc.* **2018**, *140*, 17547–17555.
44. van Dijken, D. J.; Kovaříček, P.; Ihrig, S. P.; Hecht, S. Acylhydrazones as widely tunable photoswitches. *J. Am. Chem. Soc.* **2015**, *137*, 14982–14991.
45. Ryabchun, A., Li, Q.; Lancia, F.; Aprahamian, I.; Katsonis, N. Shape-persistent actuators from hydrazone photoswitches. *J. Am. Chem. Soc.* **2019**, *141*, 1196–1200.
46. Weyandt, E.; ter Huurne, G. M.; Vantomme, G.; Markvoort, A. J.; Palmans, A. R. A.; Meijer, E. W. Photodynamic control of the chain length in supramolecular polymers:

switching an intercalator into a chain capper. *J. Am. Chem. Soc.* **2020**, *142*, 6295–6303.

47. To support the vial inversion data, we conducted the rheological experiments of the main compounds called gels. In linear dynamic mechanical tests, the storage modulus (G') for all the samples was appreciably higher that the loss modulus (G"), and G' was almost constant in a wide frequency range between 0.1 and 10 s^{-1}, thereby confirming that they are categorized into "hydrogels" without flowability. See the Supporting Information for the rheological data (Figure S2 and S10).

48. In our out-of-equilibrium pattern formation, both the photo-degradation and condensation of the peptide nanofibers occurred during the photo-irradiation. As the line width decreases, diffusion of the degraded peptide monomers/aggregates and supply of the peptide monomer from non-irradiated area would proceed in the limited area with a shorter time, resulting in the more rapid condensation of the peptide fibers. In the case of 5-μm-wide photomask, the condensation was almost completed during light irradiation. See the Supporting Information for experimental data (Figure S17).

49. Shigemitsu, H.; Kubota, R.; Nakamura, K.; Matsuzaki, T.; Minami, S.; Aoyama, T.; Urayama, K.; Hamachi, I. Protein-responsive protein release of supramolecular/polymer hydrogel composite integrating enzyme activation systems. *Nat. Commun.* **2020**, *11*, 3859.

50. Korevaar, P. A.; Georeg, S. J., Markvoor, A. J.; Smulders, M. M. J.; Hilbers, P. A. J.; Schenning, A. P. H. J.; De Greed, T. F. A.; Meijer, E. W. Pathway complexity in supramolecular polymerization. *Nature* **2012**, *481*, 492–496.

51. Ogi, S.; Sugiyasu, K.; Manna, S.; Samitsu, S.; Takeuchi, M. Living supramolecular polymerization realized through a biomimetic approach. *Nat. Chem.* **2014**, *6*, 188–195.

52. Pal, A.; Malakoutikhah, M.; Leonetti, G.; Tezcan, M.; Colomb-Delsuc, M.; Nguyen, V. D.; van der Gucht, J.; Otto, S. Controlling the structure and length of self-synthesizing supramolecular polymers through nucleated growth and disassembly. *Angew. Chem. Int. Ed.* **2015**, *54*, 7852–7856.

Methods:

The materials, instruments, experimental methods, and syntheses of the compounds are described in the Supporting Information. The experimental conditions (concentration, pH, and temperature) are described in the figure captions.

Associated contents: Synthesis, additional materials and methods and supporting data is available free of charge on the ACS Publications website.

Movies S1 to S3 (AVI file) are available free of charge on the ACS Publications website.

Author information:

*Corresponding Author: ihamachi@sbchem.kyoto-u.ac.jp

Author Contribution:

#These authors contributed equally to this work

Acknowledgments: We thank the Edanz (https://jp.edanz.com/ac) for editing a draft of this manuscript. This work was supported by a Grant-in-Aid for Scientific Research on Innovative Areas “Chemistry for Multimolecular Crowding Biosystems” (JSPS KAKENHI Grant 17H06348), the Japan Science and Technology Agency (JST) ERATO Grant Number JPMJER1802 to I.H., and by a Grant-in-Aid for Young Scientists (JSPS KAKENHI Grant 20K15400) to R.K. W.T. acknowledge JSPS Research Fellowships for Young Scientists (19J14474).

Note:

The authors declare no competing financial interests.

Table of contents artwork